Firetube model and hadron-hadron collisions

R. A. M. S. Nazareth
Instituto de Física, Universidade Federal do Rio de Janeiro, Rio de Janeiro, 21945 Brazil

T. Kodama and D. A. Portes, Jr.
Centro Brasileiro de Pesquisas Físicas, Rio de Janeiro, 22290 Brazil
(Received 17 January 1992)

A new version of the firetube model is developed to describe hadron-hadron collisions at ultrarelativistic energies. Several improvements are introduced in order to include the longitudinal expansion of intermediate fireballs, which remedies the overestimates of the transverse momenta in the previous version. It is found that, within a wide range of incident energies, the model describes well the experimental data for the single-particle rapidity distribution, two-body correlations in pseudorapidity, transverse momentum spectra of pions and kaons, the leading particle spectra, and the K/π ratio.

PACS number(s): 13.85.Ni, 12.40.Aa

I. INTRODUCTION

A couple of years ago, we proposed a simple phenomenological model for the proton-proton (antiproton) collision process [1–3] based on a mechanism in which a chromodynamical firetube fragments into intermediate fireballs which subsequently decay isotropically into the observed hadrons. The model, in spite of its simplicity, was found to reproduce the experimental rapidity and pseudorapidity distributions of pions within a wide energy interval, extending from $\sqrt{s}\sim 20$ GeV to $\sqrt{s}\sim 1$ TeV. However, there exist some shortcomings of the model because of the oversimplified picture. For example, the fireball decay was assumed to be isotropic there, and this leads to an overestimate of the transverse momenta of final pions.

Thus, we consider it worthwhile to improve this oversimplified picture of the original version, as well as to extend the model to calculate other quantities than pion rapidity distributions, such as kaon distributions and leading particle spectra. We also intend to reproduce the pion and kaon spectra in any hadron-hadron collisions other than p-p ($\bar{p}$) reactions keeping the simple geometric extension of the model.

In Sec. II, we describe the firetube model with several improvements. We first analyze the mass and rapidity distributions of fireballs and discuss them with respect to the rapidity correlations of pions. In our model, the leading particle spectra are directly related to those of the fireballs originated from the end points of the firetube. From this picture, we can calculate the leading particle spectra and the inelasticity coefficient.

We also discuss in this section the decay mode of the fireballs into hadrons. The main improvement for the treatment of the fireball decay processes is the introduction of the effect of the longitudinal expansion of the fireballs on the final hadron spectra. This remedies the large transverse momentum caused by the simple isotropic decay hypothesis used in the original version [3]. Furthermore, the kaon degree of freedom is introduced in the decay mode. For this purpose, the K/π ratio is determined as a function of the fireball mass.

In Sec. III, the results are discussed and compared with experimental data when available.

II. FIRETUBE MODEL OF HADRON-HADRON COLLISIONS

The phenomenological model developed in Refs. [1–3] describes proton-proton collisions as three-stage process. In the first part of the collision the protons become colored objects due to the exchange of their sea quarks, generating a chromodynamical flux tube (firetube) between them. This firetube can be represented by a classical string with an effective string constant. In the next stage this tube fragments into a set of intermediate objects (fireballs), which subsequently decay into the observable hadrons. This model is similar to the one developed by the Lund group [4], except that in the latter, hadrons are produced directly from the fragmentation of a string, without an intermediate fireball stage [5]. In what follows we present the main ingredients of the model in each stage.

A. Firetube formation

One of the basic characters of the model is that the effective string constant κ of the firetube is taken as a function of the impact parameter and the incident energy. The tension coefficient is given by

$$k_{\rm eff}=\epsilon_0 A(b\sqrt{s}) , \tag{1}$$

where ϵ_0 is the volumetric energy density of the flux tube with transverse area $A(b,\sqrt{s})$. The transverse area of the effective string is proportional to the total hadron-hadron cross section times a universal function of the impact parameter b [3]:

$$A(b,\sqrt{s})=\sigma_{\rm tot}(\sqrt{s})f(b) , \tag{2}$$

where

$$\frac{d^2f(b)}{d\mathbf{b}^2} \equiv \frac{1}{\sigma}\frac{d^2\sigma}{d\mathbf{b}^2} , \tag{3}$$

$A(b,\sqrt{s})$ is considered as the effective overlapping area between protons at the impact parameter b. In Ref. [3], $A(b,\sqrt{s})$ was taken just as the geometric overlapping area of two flat disks. However, from the parton point of view, the effective energy density of the string should be proportional to the numbers of partons contributing to the inelastic process. In this aspect, the universal function is rather well approximated by a Gaussian one [6] than that of the simple geometric overlap of two disks. Thus we take

$$\frac{d^2f(b)}{d\mathbf{b}^2} = \frac{\lambda}{\pi} e^{-\lambda b^2/b_{\max}^2} , \tag{4}$$

where $b_{\max}$ is related to the total inelastic cross section as

$$\pi b_{\max}^2 = \sigma_{hh}(\sqrt{s}) , \tag{5}$$

and λ is determined by the condition [6]

$$\langle b^2 \rangle = 0.47 \left[\frac{b_{\max}}{2} \right]^2 ,$$

i.e., $\lambda = 8.5$.

Then, the motion of the two colored (excited) hadrons is described by the classical Hamiltonian

$$H(b) = (p_1^2 + m_{h_1}^2)^{1/2} + (p_2^2 + m_{h_2}^2)^{1/2} + k_{\text{eff}}|x_1 - x_2| , \tag{6}$$

where x_i and p_i are the coordinates and momenta of the particles at each end of the effective string and m_{h_1} and m_{h_2} are the mass thresholds of the excited hadrons (see later). The time evolution of the system is obtained by solving the equations of motion derived from the Hamiltonian, Eq. (6). The trajectories of the end-point particles are two intertwined hyperbolas.

B. Firetube fragmentation into fireballs

Another basic ingredient of the model is the stochastic breakup of the firetube at any space-time just like in the Lund string model [4]. We denote as ω, the probability density $d^2P/(dx\,dt)$ of the firetube breakup.

The firetube breaking is related, in some way, to the spontaneous quark-antiquark pair production inside the firetube, but definitely it is not a perturbative process. It might be possible to relate ω to the energy density for the firetube from some QCD-inspired models. However we just take here the simplest choice, i.e., ω constant and consider it just a simple phenomenological parameter to fit the data.

The firetube breaking process splits the original firetube into two subfiretubes; their energy and momentum being determined by the precise point where the break takes place. This process may continue to occur in the subfiretubes. When a subfiretube does not break up within the first period of its yo-yo cycle, it collapses into a point due to the string tension. At this point, we assume that all the kinetic energy of the string in its center-of-mass (c.m.) system is converted into internal energy of a highly excited object (fireball).

For a given ω and the initial c.m. energy of the firetube, we thus can calculate analytically the mass and rapidity distributions of the fireballs [3]. However, the assumption of constancy of ω anywhere in space is obviously not appropriate near the end points of the firetube, since the boundary effects will certainly reduce the probability of breaking in order to inhibit the production of extremely short subfiretubes. In other words, we assume that the firetube breaking occurs only when the invariant mass of the resultant subfiretube is greater than or equal to some threshold value m_{th}. We consider m_{th} as a parameter of the model.

In Ref. [3] details of the firetube breakup process are discussed so that we will not repeat them here. We just show, in Fig. 1, the calculated mass and rapidity distributions of the fireballs generated by the process of the firetube breakup. Note that the form of the mass distribu-

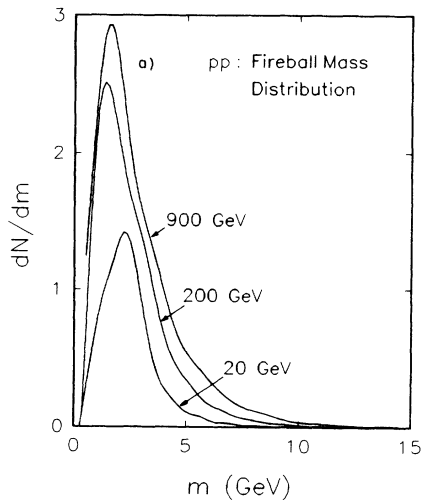

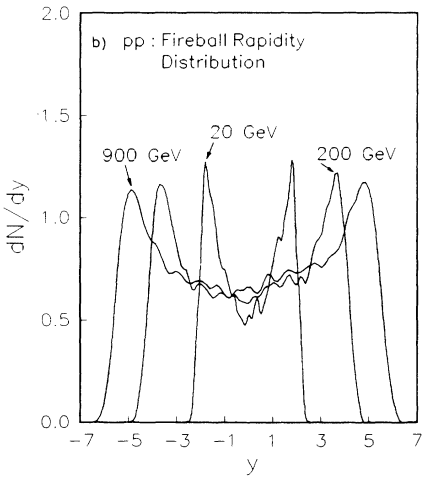

FIG. 1. (a) The mass distributions of fireballs generated by the firetube fragmentation for three different incident energies. (b) The rapidity distributions of fireballs generated by the firetube fragmentation for three different incident energies.

tion does not change appreciably with respect to the incident energy, although the higher the incident energy is, the more the heavy fireballs can appear. Consequently, the average size of fireballs increases slowly with the incident energy.

C. Correlations in rapidity of hadrons

The forms of the mass and rapidity distributions are intimately related to the correlation of the produced particles. The smallness of the average fireball mass should generate a strong correlation in the rapidity spectrum of the produced pions. In fact, phenomenological analyses of the rapidity correlation pattern of the produced particles in very-high-energy pp and $p\bar{p}$ collisions suggest the existence of some mechanism of clustering in the hadronization process [7]. Although a part of such clusters can be interpreted as hadron resonances, there seem to remain some of the correlation pattern that cannot be interpreted by hadron resonances. Since the observed hadrons are originated from these fireballs, we expect that the analysis of the two-particle correlation will provide a critical check to the mass and rapidity spectra of the fireballs predicted by the model.

The two-particle correlation in pseudorapidity space is defined as

$$C(\eta_1,\eta_2)=\frac{1}{\sigma}\frac{d^2\sigma}{d\eta_1 d\eta_2}-\frac{1}{\sigma}\frac{d\sigma}{d\eta_1}\frac{1}{\sigma}\frac{d\sigma}{d\eta_2}\ . \tag{7}$$

It is further decomposed into two parts, the so-called short-range correlation and long-range correlation as [7]

$$\begin{aligned} C_S&=\sum_n \frac{\sigma_n}{\sigma}\left[\frac{1}{\sigma_n}\frac{d^2\sigma_n}{d\eta_1 d\eta_2}-\frac{1}{\sigma_n}\frac{d\sigma_n}{d\eta_1}\frac{1}{\sigma_n}\frac{d\sigma_n}{d\eta_2}\right], \\ C_L&=\sum_n \frac{\sigma_n}{\sigma}\left[\frac{1}{\sigma}\frac{d\sigma}{d\eta_1}-\frac{1}{\sigma_n}\frac{d\sigma_n}{d\eta_1}\right] \\ &\quad\times\left[\frac{1}{\sigma}\frac{d\sigma}{d\eta_2}-\frac{1}{\sigma_n}\frac{d\sigma_n}{d\eta_2}\right], \end{aligned} \tag{8}$$

where the subscript n indicates the quantity of given multiplicity n. It has been argued that the observed short-range correlation pattern (see Fig. 2) suggests the existence of clusters at the time of the hadronization. Since the short-range correlation is sensible to the size of clusters, this will provide a good check of the mass distribution of the fireballs of our model. In order to see this effect, we calculated here the rapidity correlation of pions based on the fireball spectrum of the present model. The whole process of p-p and p-$\bar{p}$ collisions are simulated by the Monte Carlo method. The momenta of the final hadrons are generated according to the isotropic fireball decay [3]. The multiplicity distribution of hadrons of a fireball is taken to be a Poisson type with average multiplicity $\langle n\rangle=2.1\sqrt{M}$ where M is the fireball mass. In Fig. 2, we compare the results to the experimental data for $\sqrt{s}$ between 63 and 900 GeV. The solid lines are the results of the model, and the filled circles are the experimental values [8]. We see the short-range correlations are surprisingly well reproduced by the model for all energies. It is worthwhile to mention that in these calculations, no new adjustable parameters are introduced. We thus conclude that the present picture of the formation of intermediate fireballs with the predicted mass distribution of the firetube model is consistent to the short-range rapidity correlation data. Furthermore, in the present model fireballs play a similar role of clusters used to explain the forward-backward correlations in multiplicity data [9]. Thus, together with the leading particle effect which is described below, we expect that the present model should also explain these long-range correlations in multiplicity.

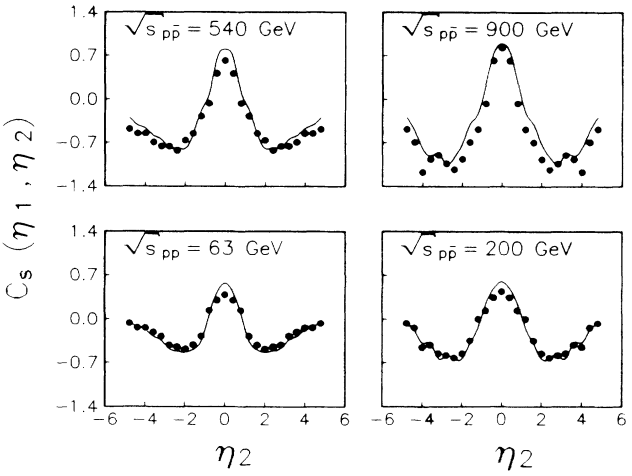

FIG. 2. Short-range correlations in pseudorapidity, $C_s(\eta_1,\eta_2)$ for various incident energies, plotted as functions of η_2, with $\eta_1=0$. Data points are taken from Ref. [8].

On the other hand, the long-range correlation in rapidity spectrum is intimately related to the multiplicity fluctuations [7]. In the present calculation, we simply assumed the Poisson distribution of the multiplicity distribution for the fireball decay. In this case, it is found that the total fluctuation in multiplicity of pions became smaller than the experimental one. This leads to an overall underestimate of the normalization factor in the long-range correlation spectra, but its functional form is well reproduced [10]. If we take other distributions than Poisson type, which give larger fluctuations in multiplicity for each fireball decay, the long-range correlations are also well reproduced.

We also checked the influence of anisotropic decay of fireballs into pions on the correlation data [10]. We found that a longitudinally deformed decay mode improves the long-range correlation data. This also improves the overestimate of average transverse momenta of produced pions as already pointed out in Ref. [1]. Therefore, it seems crucial to include the effect of longitudinal expansion of fireballs before they hadronize into hadrons. This will be discussed later in detail.

D. Leading particle spectra

In our model, the incident hadrons are always attached to the fireballs at the end points of the original firetube. Thus, the leading particle spectra are intimately related to the mass and rapidity distributions of these end-point

fireballs.

If we let w to be the probability of firetube breaking per unit time, $\sqrt{s}$ the initial center-of-mass energy, m the fireball mass, and y the fireball rapidity, then the end-point fireball spectra, in the limit $\sqrt{s} \gg m_h$, are given by

$$\left[\frac{d^2P}{dm\,dy}\right]_{\mathrm{EP}} = \frac{mw}{k_{\mathrm{eff}}^2}\exp\left[-\frac{wm\sqrt{s}}{2k_{\mathrm{eff}}^2}e^{\mp y}\right]\Theta(\mp y + y_{\max}) , \tag{9}$$

where the minus and plus signs of y refer to the fireball from the right and left, respectively, $y_{\max} = \ln(\sqrt{s}/m)$, and Θ is the Heaviside function. The rapidity distribution of the end-point fireball can be obtained by integrating the above expression with respect to m. In practice, the finiteness of m_{th} (we took in this work $m_{\mathrm{th}} \simeq 1$ GeV) alters the spectrum especially for low incident energies. In Fig. 3, we show the rapidity distribution of the end-point fireballs for different incident energies. For higher energies, the distribution tends to that of Eq. (9).

In order to relate the fireball spectrum to that of the leading particle, we assume that the incident protons are detached from the fireball before the system enters in the thermal equilibrium if the mass of the fireball is not so large, say $m \leq m_l$. Such a process can be simulated by a mechanism similar to that of firetube breakup, except that the breaking occurs just at the position of the leading particle trajectory, leaving the minimum mass m_{th} for the remnant fireball. For $m > m_l$, we calculate the proton spectra with the prescription which is described later. However, the leading particle spectra are rather insensitive on the details of these decay modes, but essentially just depend only on the value of m_l, which was adjusted as $\simeq 6$ GeV to reproduce the experimental data. In Fig. 4, we show the calculated leading particle spectrum, together with the experimental values [11–13]. Adding the contribution from the diffractive process (dashed curve), the accordance between the calculated and the experimental spectra is fairly good. The diffractive contribution here is supposed to be 20% of the total inelastic cross section. From this leading particle spectrum, we can calculate the inelasticity coefficient, defined as $1-\langle E\rangle/E_0$, where $\langle E\rangle$ is the average value of the final proton energy and E_0 the incident energy. In Fig. 5, we show the calculated inelasticity as a function of the incident energy. As can be seen from this figure, our model predicts the slow increase of the inelasticity coefficient with the incident energy. This behavior is analogous to the dual string model [14,15] (see also the discussions in Refs. [16] and [17]).

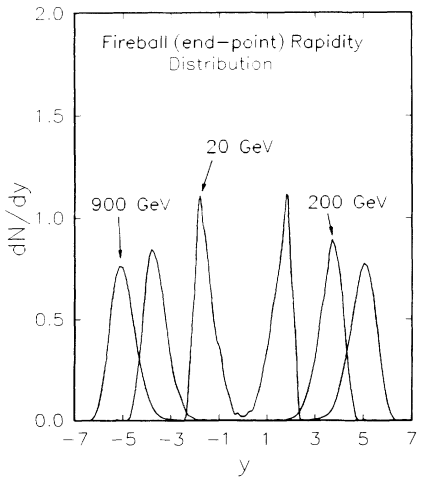

FIG. 3. The rapidity distribution of fireballs at the end points of the firetube for three different incident energies.

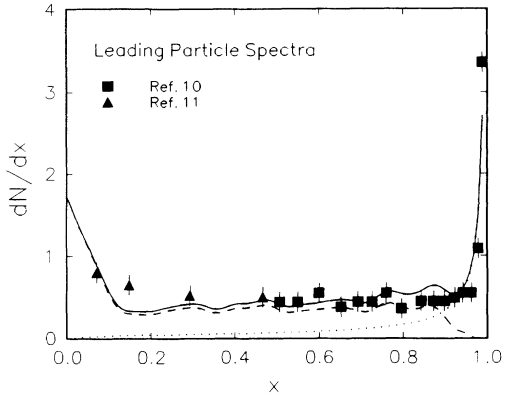

FIG. 4. Leading particle spectra plotted as a function of the Feynman variable x_F, defined as $x_F = p_\parallel/p_0$, where $p_\parallel$ and p_0 are, respectively, the final and initial proton longitudinal momenta. The dashed line is the result obtained by our model ($\sqrt{s} = 20$ GeV). The dotted line shows the contribution of the diffractive process. The solid curve corresponds to the sum of these two contributions. Triangles and squares are data points [11,12].

E. Longitudinal expansion of fireball

The hadron spectrum is calculated from the decay of the fireballs as the final stage of the model. Several alternative assumptions may be made to treat decay processes. In Ref. [3] a statistical thermal model was considered. According to it, the pion and kaon spectra, in the center-of-mass of a fireball with mass m, are, respectively, given by

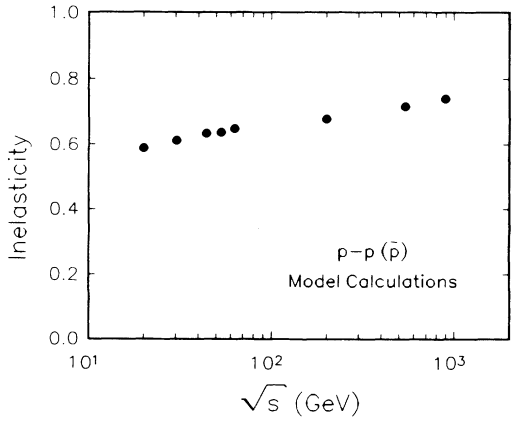

FIG. 5. Inelasticity coefficient as a function of the incident energy.

$$\frac{1}{\sigma_\pi}\frac{d^3\sigma_\pi}{dp^3}=\frac{Z_\pi}{\pi}e^{-E_t\cosh(y)/T(m)}, \tag{10}$$

$$\frac{1}{\sigma_\kappa}\frac{d^3\sigma_\kappa}{dp^3}=\frac{Z_\kappa}{\pi}e^{-E_t\cosh(y)/T(m)}, \tag{11}$$

where $E=E_t\cosh(y)$ and p are the energy and momentum of the emitted particles and $Z_{\pi,\kappa}$ is the normalization constant.

Here, the "temperature" T of a fireball should be considered as an effective one in the sense that it does not necessarily correspond to the real temperature at the time when the fireball dissociates into final free hadrons. It is merely a parameter which represents the exponential decay of the transverse spectra of the final particles, and therefore many other nonthermal effects are possibly incorporated in this parameter, such as transverse expansion, final state interactions, and nonequilibrium components. In fact, Hama and Navarra [18] argued that, while the actual dissociation temperature decreases as the mass of the fireball increases, the average transverse momenta of final particles can increase due to the fluid dynamical effect of transverse expansion.

The effective temperature is parametrized as a function of the fireball mass by [3]

$$T=\frac{m_\pi}{1-1.6v}, \tag{12}$$

where

$$v=\frac{1.2(m^\nu-m_{\rm th})}{m^\nu+\sqrt{m^{2\nu}-2.24m_{\rm th}^\nu(m^\nu-m_{\rm th}^\nu)}}, \tag{13}$$

which simulates the behavior of the transverse momentum $\langle p_T\rangle$ as a power function of the fireball mass [19] with an exponent ν. Here we take ν as an adjustable parameter.

In order to treat the longitudinal expansion of the fireball, we suppose that the final hadron spectra are obtained as a convolution of the collective motion of the fireball elements and the thermal decay spectra of hadrons, like in the hydrodynamical model. In this case, the rapidity distribution of the fluid elements of the fireball can be well approximated by a Gaussian distribution [20],

$$f(\bar{y})\propto e^{-1/2\alpha\bar{y}^2}, \tag{14}$$

which in turn can be approximated by

$$f(\bar{y})=\frac{1}{2K_0(\alpha)}e^{-\alpha\cosh(\bar{y})}, \tag{15}$$

where K_0 is the Bessel function, $\bar{y}$ stands for the rapidity of the fluid element, and α is a parameter related to the longitudinal energy of the fluid in the fireball.

The longitudinal expansion in the hydrodynamical model is relatively well studied, and we took the dependence of the parameter α on the fireball mass as

$$\alpha=\frac{2}{\ln(m/m_0)}, \tag{16}$$

where m_0 denotes the mass scale for which the longitudinal expansion starts.

In our model, the different firetube thickness can cause the formation of different fireballs with same mass m. A fireball formed from a thinner firetube has larger longitudinal kinetic energy than that with the same mass which is formed from a thicker firetube. Then, we expect that the former one should have the larger longitudinal expansion than the latter. In this mode, the parameter m_0 should be related to some quantity which measures how the initial condition for the formation of a fireball is elongated.

We then define the parameter m_0 as the mass of the firetube whose initial longitudinal dimension L and transversal dimension R are related as

$$\alpha_0=\frac{L}{R},$$

where α_0 is a parameter independent of the firetube. Since the longitudinal size L is given by

$$L\simeq\frac{m_0}{\epsilon_0 A(b,\sqrt{s})},$$

whereas the transversal size is given by

$$R\simeq\left[\frac{A(b,\sqrt{s}}{\pi}\right]^{1/2},$$

we get

$$m_0=\alpha_0\epsilon_0 A^{3/2}(b,\sqrt{s}). \tag{17}$$

F. Hadron spectra

Once the temperature parameter T and the longitudinal expansion coefficient α are determined as a function of the fireball mass m, we calculate the pion spectra as

$$\frac{1}{\sigma\pi}\frac{d^3\sigma_\pi}{dp^3}=\frac{Z_\pi}{\pi}\int_{-\infty}^{+\infty}d\bar{y}\frac{1}{2K_0(\alpha)}e^{-\alpha\cosh(\bar{y})}e^{-E_t\cosh(y-\bar{y})/T(m_f)}$$
$$=\frac{Z_\pi}{K_0(\alpha)}K_0\left[\left[\alpha^2+2\left[\frac{E_T}{T}\right]\alpha\cosh(y)+\left[\frac{E_T}{T}\right]^2\right]^{1/2}\right], \tag{18}$$

where E_T is the transverse energy. For kaons and baryons, we have analogous expressions.

Note that for large α we recover the isotropic decay inclusive spectrum, i.e.,

$$\frac{Z_\pi}{K_0(\alpha)}K_0\left[\left[\alpha^2+2\left[\frac{E_T}{T}\right]\alpha\cosh(y)+\left[\frac{E_T}{T}\right]^2\right]^{1/2}\right]_\infty\rightarrow\frac{Z_\pi}{\pi}e^{-E_t\cosh(y)/T(m)}. \tag{19}$$

For a given mass m, the average multiplicity $\bar{N}$ is determined by the normalization condition

$$\bar{N}_{\pi,\kappa,B}=\sum_{\pi,\kappa,B}\int d^3\mathbf{p}\frac{1}{\sigma}\frac{d^3\sigma}{dp^3}$$
$$=4Z_{\pi,\kappa,B}m_{\pi,\kappa,B}TK_1(m_{\pi,\kappa,B}/T) \quad (20)$$

and the energy conservation

$$m=\sum_{\pi,\kappa,B}\int d^3\mathbf{p}\frac{E}{\sigma}\frac{d^3\sigma}{dp^3}$$
$$=\frac{4K_1(\alpha)}{K_0(\alpha)}[Z_\pi m_\pi^2 TK_2(m_\pi/T)+Z_\kappa m_\kappa^2 TK_2(m_\pi/T)$$
$$+Z_B m_B^2 TK_2(m_B/T)], \quad (21)$$

where the subscripts π, κ, and B refer to pions, kaons, and baryons, respectively. Neglecting baryon production in the decay process, we have $N_B=1$ for the fireball formed at the end points of the initial firetube, and $N_B=0$ for other fireballs in between. This simplification allows us to determine the normalization constant Z_B from Eq. (20). We have left with three equations for the four unknown variables, $N_\pi, N_\kappa, Z_\pi, Z_\kappa$. It is necessary to specify the relative abundance of kaons to pions. To determine the relative normalization of pions and kaons as a function of the fireball mass, we note that the K/π ratio should vanish for $m\to 2m_\kappa$, and should tend asymptotically to some constant for $m\to\infty$. Thus, we introduce the ansatz

$$\frac{Z_\kappa}{Z_\pi}=\left[\frac{Z_\kappa}{Z_\pi}\right]_\infty\left[1-\exp\left[\frac{m-2m_\kappa}{\xi}\right]\right], \quad (22)$$

where $(Z_\kappa/Z_\pi)_\infty$ and ξ are taken as adjustable parameters.

With the help of the normalization conditions Eqs. (20)–(22), together with the condition $N_B=0$ or $N_B=1$, the hadron spectra from a fireball of a given mass m can now be calculated completely [Eq. (18) and analogous expressions for kaons and baryons].

The rapidity (y) and the transverse momentum (p_t) distributions of hadrons from a fireball are respectively calculated by

$$\frac{dN_{\pi,k}}{dy}=\int\frac{d^2N_{\pi,k}}{dy\,dp_t^2}dp_t^2,$$
$$\frac{dN_{\pi,k}}{dp_t^2}=\int\frac{d^2N_{\pi,k}}{dy\,dp_t^2}dy. \quad (23)$$

With the above prescriptions for the decay of a fireball, the final-hadron spectra are then calculated by folding the fireball mass and rapidity distributions as

$$\frac{dN_{\pi,k}}{dy}=\int_{m_{\rm th}}^{m_{\rm max}}dm\int_{-y_{\rm max}}^{y_{\rm max}}dy_{\rm FB}\frac{dN}{dy_{\pi,k}}\frac{d^2P}{dm\,dy_{\rm FB}} \quad (24)$$

and

$$\frac{dN_{\pi,k}}{dp_t^2}=\int_{m_{\rm th}}^{m_{\rm max}}dm\int_{-y_{\rm max}}^{y_{\rm max}}dy_{\rm FB}\frac{dN}{dp_{t^2_{\pi,k}}}\frac{d^2P}{dm\,dy_{\rm FB}}. \quad (25)$$

The average total multiplicity of hadrons n_π and n_k are given by

$$n_\pi=\int_{m_{\rm th}}^{m_{\rm max}}dm\langle n_\pi(m)\rangle\frac{dP}{dm_{\rm FB}},$$
$$n_k=\int_{m_{\rm th}}^{m_{\rm max}}dm\langle n_k(m)\rangle\frac{dP}{dm_{\rm FB}}. \quad (26)$$

G. Charged particles

Formulas in the preceding section refer to the hadron spectra without distinction of charged states. However, the experimental data are usually concerned with the charged particles, only. Therefore, it is necessary to convert our formulas to those for the charged particles. For this purpose, we simply assume that the fireballs which do not contain the incident proton carry always zero total charge, and that any charge state of mesons (pions and kaons) has the same probability. Thus, for these fireballs, we have

$$N_{\pi^\pm}=N_{\pi^0}=\tfrac{1}{3}N_\pi,$$
$$N_{K^\pm}=N_{K^0}=N_{\bar{K}^0}=\tfrac{1}{4}N_K. \quad (27)$$

For the fireballs which contain the incident protons, we assume that the proton transfers a half of its charge, in average, to mesons. The final charge configuration can be determined by maximizing the number of ways of distributing this transferred positive charge between π^+ and K^+ under the constraints,

$$N_{\pi^+}+N_{\pi^-}+N_{\pi^0}=N_\pi,$$
$$N_{K^+}+N_{K^0}=N_{K^-}+N_{\bar{K}^0}=\tfrac{1}{2}N_K, \quad (28)$$
$$N_{\pi^+}-N_{\pi^-}=Q,$$

where Q is the transferred charge ($=\frac{1}{2}$). We found that the above condition leads to

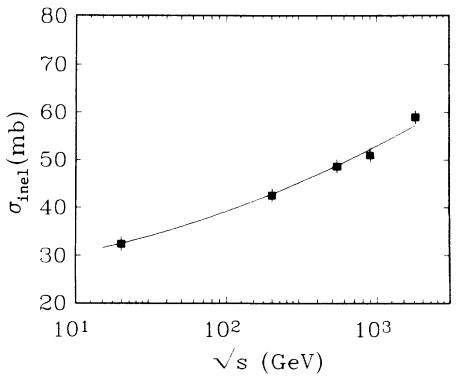

FIG. 6. Inelastic p-p ($\bar{p}$) cross section as a function of the incident energy. The solid curve corresponds to Eq. (25). Experimental data are taken from Refs. [21–23].

TABLE I. Parameters for firetube.

Parameter	Physical role	Expression
ϵ_0	Volumetric energy density per parton	Eq. (1)
ω	Probability density of firetube breaking	Eq. (9)
m_{th}	Threshold mass of fireballs	Eq. (26)

$$
\begin{aligned}
&N_{\pi^0} \simeq \tfrac{1}{3} N_\pi \ , \\
&Q^* = Q\left[1-\tfrac{1}{2}\frac{N_K}{N^\pi}\right] , \\
&N_{\pi^+} = \tfrac{1}{2}(N_\pi + Q^* - N_{\pi^0}) \ , \\
&N_{\pi^-} = \tfrac{1}{2}(N_\pi - Q^* - N_{\pi^0}) \ , \\
&N_{K^+} = \tfrac{1}{4}(N_\pi + Q) \ , \\
&N_{K^+} = \tfrac{1}{4}(N_\pi - Q) \ .
\end{aligned}
\tag{29}
$$

III. RESULTS AND DISCUSSION

In the present model, the incident energy dependence of the observable quantities enters only through that of the total inelastic cross section, $\sigma_{\text{inel}}(\sqrt{s})$ (geometrical scaling [3]). In the present analysis, we fitted the experimental values [21–23] of the cross section (see Fig. 6) as a function of $\sqrt{s}$ as

$$\sigma_{\text{inel}} = 26.55 + 0.577 \ln\sqrt{s} + 0.47(\ln\sqrt{s})^2 \ . \tag{30}$$

After fixing the total cross section, we search the values of the parameters introduced in the previous section to fit the various observable quantities, such as total multiplicity, rapidity distribution, transverse momenta, K/π ratio, etc.

For the sake of bookkeeping, we list in Tables I and II the parameters of the model and their physical meaning. These parameters are classified into two groups: one for the firetube dynamics and other the fireball decay into hadrons.

It is worthwhile to mention that there exists a scaling relation [3] among the parameters $\epsilon, \omega, m_{\text{th}}$ and the incident energy $\sqrt{s}$. In particular for higher energies, where the role of m_{th} becomes ineffective, the first two parameters are almost reduced into one parameter ω/ϵ^2.

However, among these parameters, we simply fixed *a priori* the two of them: $\omega = 0.01$ fm^{-2} and $m_{\text{th}} = 1$ GeV. This is because some of the observable quantities are not sensible to these parameters. Furthermore, for change of these parameters within a reasonable interval, we can always obtain the same good results as before by adjusting the others. Therefore, we use just the five parameters ϵ_0, α_0, ν, $(Z_\kappa/Z_\pi)_\infty$, and ξ to fit the K/π ratio, the (pseudo) rapidity distributions and transverse momentum spectra. The first one ϵ_0 is the only parameter related to the firetube fragmentation. The parameters ϵ_0 and α_0 are found to control essentially the overall multiplicity data, together with the temperature parameter ν. This last parameter strongly affects the P_t distributions, as expected. To have a reasonable behavior of the P_t spectra, we obtained the value

$$\nu \simeq 1/5 \ .$$

Once the temperature parameter is fixed to the above value, we adjusted the parameters ϵ_0, α_0, $(Z_\kappa/Z_\pi)_\infty$, and ξ to reproduce the experimental data. We found that the following values reproduce the overall behavior of the experimental data:

$$
\begin{aligned}
&\epsilon_0 = 0.3 \ , \\
&\alpha_0 = 0.02 \ , \\
&\left[\frac{Z_\kappa}{Z_\pi}\right]_\infty = 0.15 \ , \\
&\xi = 2.4 \ .
\end{aligned}
$$

In the following, we present the results calculated with the above values of the parameters.

A. Rapidity (pseudorapidity) distribution

The basic change introduced in this new version of the firetube model compared to the original one [3] is the longitudinal expansion of the fireballs. Since the transverse energies are much smaller than the longitudinal ones, we expect that this change will not influence much the rapidity spectra. In fact, as shown in Figs. 7(a) and 7(b), the rapidity (or pseudorapidity) distributions stayed as good as in Ref. [3] reproducing well the experimental data [22–26] for all values of $\sqrt{s}$ from 20 to 900 GeV.

For higher energies, only the pseudorapidity experimental distributions are available. For the sake of direct comparison, we converted our calculated rapidity spectra into those for pseudorapidity, using the approximate formula [27]

TABLE II. Parameters of fireball decay.

Parameter	Physcial role	Expression
α_0	Mass scale parameter for longitudinal expression	Eq. (17)
ν	Mass dependence of the temperature $T(m)$	Eq. (13)
$\left[Z_\kappa/Z_\pi\right]_\infty$, ξ	Mass dependence of the K-π ratio	Eq. (22)

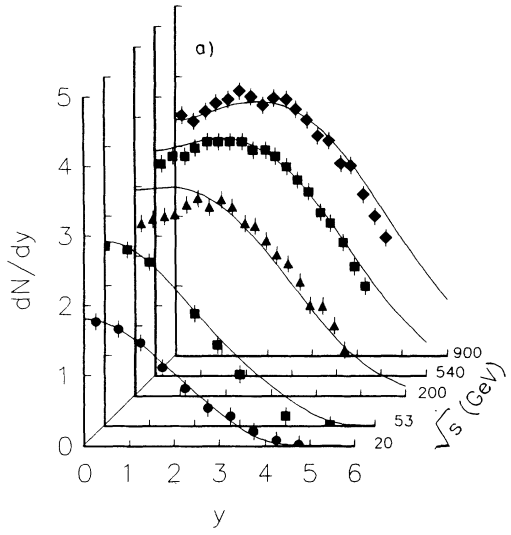

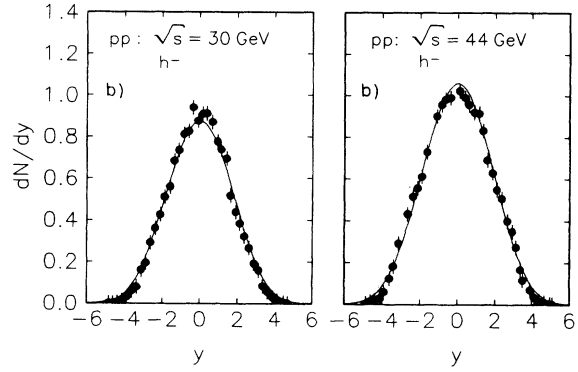

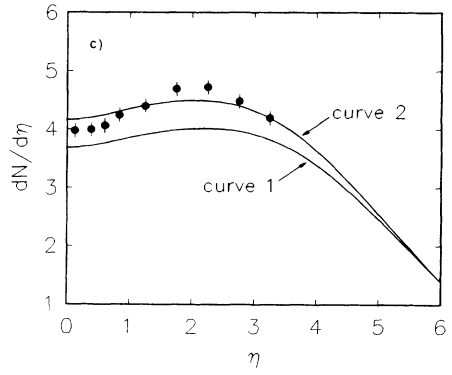

FIG. 7. (a) (Pseudo) rapidity distributions of charged particles for various energies. The two lowest energy cases ($\sqrt{s}=20,53$ GeV) refer to the rapidity distributions, whereas the remaining cases ($\sqrt{s}=200,540,900$ GeV) refer to the pseudorapidity distributions. Data points are taken from Refs. [22–25]. (b) Rapidity distributions of negatively charged particles for energies $\sqrt{s}=30$ and 44 GeV. Data points are taken from Ref. [26]. (c) Pseudorapidity distribution of charged particles for $\sqrt{s}=1800$ GeV. The curve 1 is the result obtained with the experimental inelastic cross section. The curve 2 corresponds to the result obtained with the value of the inelastic cross section 10% higher. Data points are taken from Ref. [28].

$$\frac{dN}{d\eta}=\left[1-\frac{m^2}{\langle E_t^2\rangle \cosh y^2}\right]^{1/2}\frac{dN}{dy},$$

with

$$\eta=\tfrac{1}{2}\ln\frac{\cosh y\left[1-\dfrac{m^2}{\langle E_t^2\rangle\cosh y^2}\right]^{1/2}+\sinh y}{\cosh y\left[1-\dfrac{m^2}{\langle E_t^2\rangle\cosh y^2}\right]^{1/2}-\sinh y},$$

where $\langle E_t^2\rangle$ is the average transverse energy (see below).

For $\sqrt{s}=1800$ GeV, the pseudorapidity distribution in the central region is found to be lower than the experimental data [28] [Fig. 7(c), curve 1]. If we would have taken the inelastic cross section higher for about 10%, we could again well reproduce the data [Fig. 7(c), curve 2]. In our model, the effective energy density of the firetube is simply proportional to the numbers of partons contributing to the inelastic process. It seems that processes such as hard QCD processes with transverse momentum scales $p_T \geq 2$ GeV/c should explicitly be taken into account. Some further investigation is necessary to understand this point.

B. Transverse momenta

In Fig. 8, we plotted the calculated $\langle p_T\rangle$ as a function of the incident energy which shows an excellent agreement with the experimental data [29–32] for pions, although the agreement with the kaon data is not so good. In particular, a kind of discontinuity observed in the kaon data around $\sqrt{s}\sim 200$ GeV is difficult to be reproduced in the present model. Note that the slow increase of $\langle p_T\rangle$ for higher energies reflects the increase of the average fireball mass.

Figures 9(a)–9(d) show the comparison of the calculated spectra of pions and kaons with the corresponding experimental data. In all cases, the agreement is excellent.

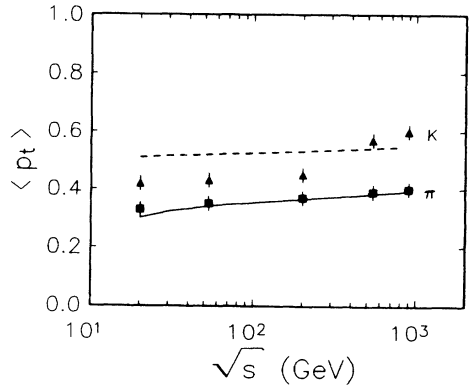

FIG. 8. Average transverse momentum of produced particles as a function of the incident energy. The solid curve (calculated) and the squares (experimental) refer to pion data. The dashed curve (calculated) and the triangles (experimental) refer to kaon data.

C. Kaon to pion ratio

Figure 10 shows the comparison of the calculated K/π ratio with the experimental data [31] as a function of the incident energy. In our model there are essentially two parameters, $(Z_\kappa/Z_\pi)_\infty$, ξ to control this quantity. However, the ansatz Eq. (22) refers to the dependence of the ratio as a function of the fireball mass, not the incident energy. Thus, the final value of the ratio depends on the mass distribution of the fireballs, which in turn reflects the dependence on the incident energy. The agreement of our curve to the experimental values is excellent.

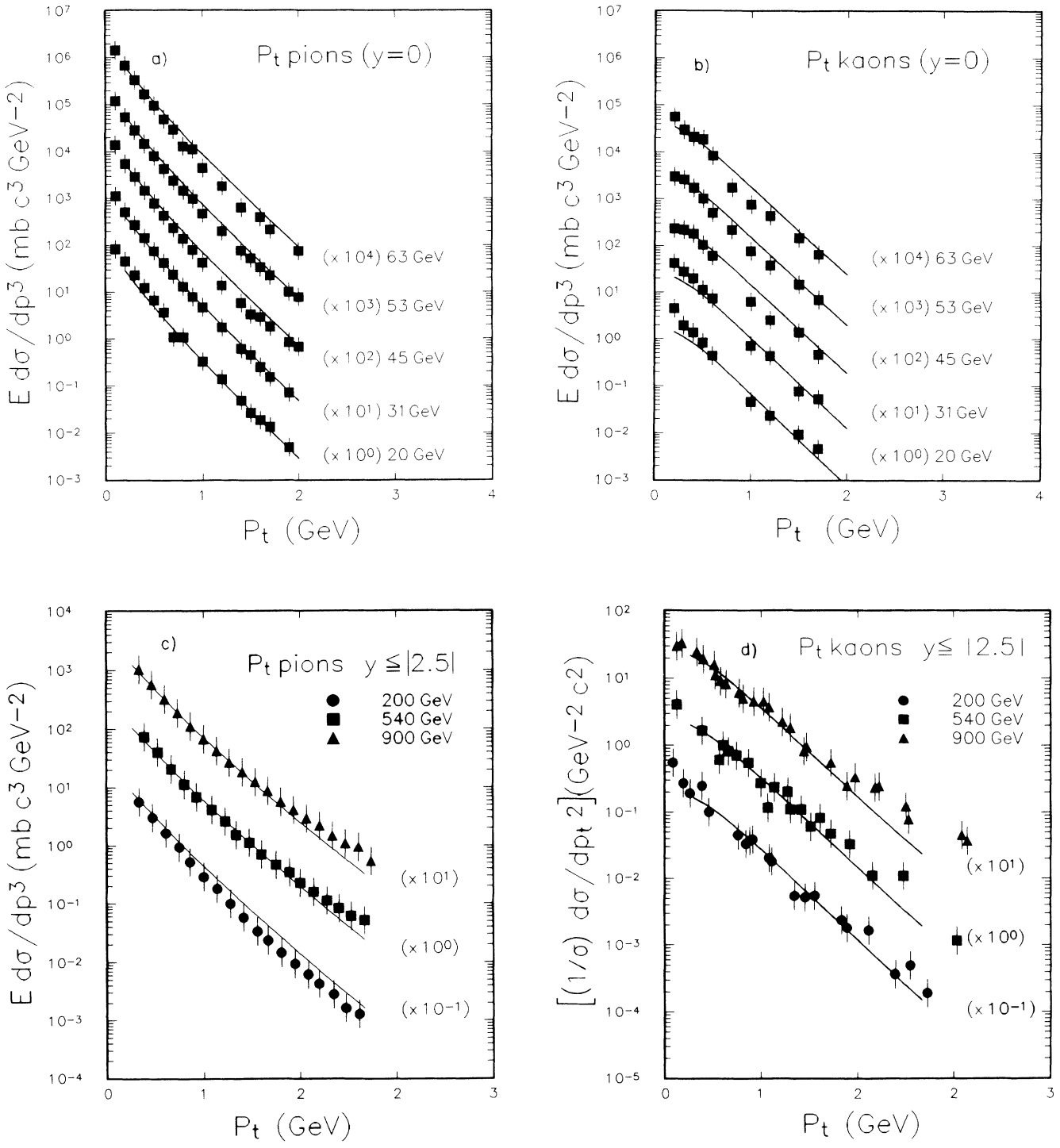

FIG. 9. (a) Pion spectra at $y=0$ plotted as function of P_t. (b) Kaon spectra at $y=0$ plotted as function of P_t. (c) Pion spectra, averaged in the rapidity interval $-2.5<y<2.5$, plotted as functions of P_t. (d) Kaon spectra, integrated in the rapidity interval $-2.5<y<2.5$, plotted as function of P_t.

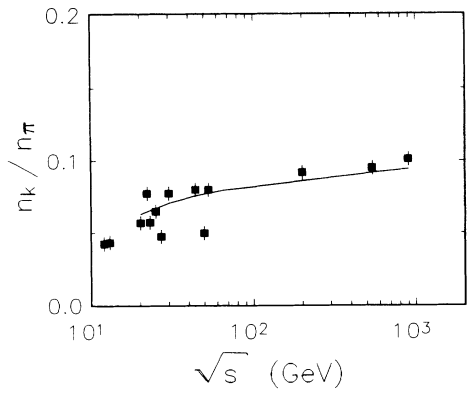

FIG. 10. K/π ratio plotted as a function of the incident energy. The solid curve is the result of the calculation. The squares are the experimental data of Ref. [31].

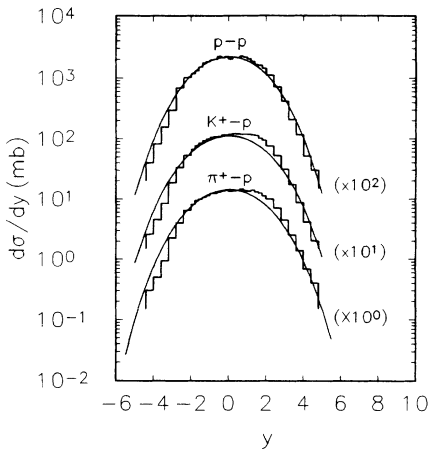

FIG. 11. Rapidity distributions of negative charged particles for $p+p$ (solid curve), $\pi^+ + p$ (dashed curve), and $K^+ + p$ (dash-dotted curve) reactions at $p_{\text{lab}} = 250$ GeV/c. The histograms represent the experimental data [33].

D. Hadron-proton collisions

It is interesting to apply our model to another hadron-hadron collision processes than that of the proton-(anti)proton case. Here, we calculate the rapidity distribution of negative pions for the pion-proton, kaon-proton, and proton-proton collisions at $p_{\text{inc}} = 250$ GeV/c. In the present calculation, the only change introduced for the K-p and π-p cases was to use the value of the experimental inelastic cross sections [21] for each reaction, instead of the formula Eq. (25). All other values of the parameters are kept equal to those of the previous results. Figure 11 is the calculated rapidity distribution of negative charged particles, compared with the experimental data [33]. The agreement for proton-proton case is very good as expected. For the pion-proton reaction, the overall behavior of the rapidity distribution is well reproduced by the simple substitution of the cross section value in our model, except for the small asymmetry. For the kaon-proton reaction, our result becomes less satisfactory. These calculations suggest that the influence of the valence quarks, especially those of strange (heavy) quarks, seems to violate the idea of the simple geometrical scaling at such lower energies. In the present model, the roles of the valence quarks are completely neglected.

IV. CONCLUDING REMARKS

In this paper, we develop some improvements of the firetube model. The main point is the introduction of the longitudinal expansion effect of the fireballs, which improves the behavior of the transverse momenta of the final hadrons. The present version is found to reproduce almost all the global properties of the experimental inclusive observables of proton-(anti)proton reactions. Some semi-inclusive data, such as the two-particle correlations in pseudorapidity space, are also reproduced in this model. With a trivial extension of the model, it also reproduces the data for the pion-proton case.

We also expect that the extension of the present model to more complex systems, such as p-nucleus or light-nucleus–nucleus reactions, will serve to describe the macroscopic aspects of the hadron productions, in particular, their peripheral collisions. These calculations are now in progress.

Several points deserve to be commented. We remind ourselves that the present model is concerned mainly with the macroscopic properties of the observable quantities, particularly with their dependence on the incident energy, without entering into the details of the incident hadron structure. All of these energy dependences come out as a consequence of the energy dependence of the total inelastic cross section. We found that most of the data treated here fit with this vision, changing smoothly with the incident energy. However, some of them seem to be out of this scheme. The first one is the average transverse momenta of kaons. As is seen from Fig. 8, there seems to exist some abrupt change around $\sqrt{s} \sim 200$ GeV. This discontinuous behavior is also seen in the form of pseudorapidity distribution at this energy. Another one is the data at $\sqrt{s} = 1800$ GeV. The inelastic cross section value at this energy fails to fit the observed pseudorapidity distribution. Some further investigation is necessary to understand these points.

[1] N. Prado, R. A. M. S. Nazareth, and T. Kodama, Rev. Bras. Fis. **16**, 452 (1986).
[2] N. Prado, Ph.D. thesis, Institute of Physics, UFRJ, 1989.
[3] R. A. M. S. Nazareth, N. Prado, and T. Kodama, Phys. Rev. D **40**, 2861 (1989).
[4] X. Artru and G. Mennesier, Nucl. Phys. **B70**, 93 (1971); B. Andersson, G. Gustafson, G. Ingelman, T. Sjöstrand, and X. Artru, Phys. Rev. **97**, 31 (1983).
[5] A two-step mechanism was also suggested for e-$\bar{e}$ jet phenomena by T. D. Gottschalk, Nucl. Phys **B239**, 349 (1984).
[6] F. E. Low, Phys. Rev. D **12**, 163 (1975).
[7] E. L. Berger, Nucl. Phys. **B85**, 61 (1975).
[8] UA5 Collaboration, G. J. Alner *et al.*, Phys. Rep. **154**, 247 (1987); R. Singer *et al.*, Phys. Rev. D **16**, 1261 (1977); S. R.

Amendolia *et al.*, Nuovo Cimento **31A**, 17 (1976); UA5 Collaboration, R. E. Ansorge *et al.*, Z. Phys. C **37**, 191 (1988).
[9] S. Uhlig *et al.*, Nucl. Phys. **B132**, 15 (1978).
[10] D. A. Portes, Jr., thesis, Centro Brasileiro de Pesquisas Fisicas, Rio de Janeiro, 1991.
[11] P. Cappilupi *et al.*, Nucl. Phys. **B70**, 1 (1974).
[12] J. W. Chapman *et al.*, Phys. Rev. Lett. **32**, 257 (1974).
[13] M. Basile *et al.*, Lett. Nuovo Cimento **38**, 359 (1983).
[14] A. Kaidalov and K. A. Ter Matrirusian, Phys. Lett. **117B**, 247 (1982).
[15] S. Barshay and Y. Chiba, Phys. Lett. **167B**, 449 (1986).
[16] J. N. Capedevielle, J. Phys. G **15**, 909 (1989).
[17] A. Ohsawa and K. Sawayanagai, Phys. Rev. D **45**, 3128 (1992).
[18] Y. Hama and F. S. Navarra, Z. Phys. C (to be published).
[19] G. A. Kilekhin, Zh. Eksp. Teor. Fiz. **35**, 1185 (1958) [Sov. Phys. JETP **8**, 829 (1959)].
[20] Y. Hama, Phys. Rev. D **19**, 2623 (1979).
[21] NA22 Collaboration, M. Adamus *et al.*, Z. Phys. C **32**, 475 (1986).
[22] UA5 Collaboration, G. J. Alner *et al.*, Phys. Rep. **154**, 247 (1987).
[23] UA5 Collaboration, G. J. Alner *et al.*, Z. Phys. C **33**, 1 (1986).
[24] C. De Marzo *et al.*, Phys. Rev. D **26**, 1019 (1982).
[25] A. Breakstone *et al.*, Phys. Lett. **132B**, 458 (1983).
[26] W. Bell *et al.*, Z. Phys. C **27**, 191 (1985).
[27] C.-Y. Wong, Phys. Rev. D **32**, 94 (1985).
[28] F. Abe *et al.*, Phys. Rev. D **41**, 2330 (1990).
[29] G. J. Alner *et al.*, Nucl. Phys. **B258**, 505 (1985).
[30] B. Alper *et al.*, Nucl. Phys. **B100**, 237 (1975).
[31] R. E. Ansorge *et al.*, Phys. Lett. B **199**, 311 (1987).
[32] G. Arnison *et al.*, Phys. Lett. **118B**, 167 (1982).
[33] EHS-NA22 Collaboration, M. Adamus *et al.*, Z. Phys. C **39**, 311 (1988).